doi:10.1016/j.jmb.2004.07.015 J. Mol. Biol. (2004) xx, 1–17

JMB

Available online at www.sciencedirect.com

SCIENCE DIRECT®

ELSEVIER

Exploring the Structural Dynamics of the *E. coli* Chaperonin GroEL Using Translation-libration-screw Crystallographic Refinement of Intermediate States

Charu Chaudhry[1], Arthur L. Horwich[2], Axel T. Brunger[3] and Paul D. Adams[4]*

[1]*Department of Molecular Biophysics and Biochemistry Yale University, New Haven CT 06520, USA*

[2]*Department of Genetics and Howard Hughes Medical Institute, Yale University New Haven, CT 06510, USA*

[3]*Department of Molecular and Cellular Physiology, Neurology and Neurological Sciences and Stanford Synchrotron Radiation Laboratory and Howard Hughes Medical Institute, Stanford University Stanford, CA 94305, USA*

[4]*Lawrence Berkeley National Laboratory, One Cyclotron Road BLDG 4R0230, Berkeley, CA 94720-8235, USA*

**Corresponding author*

Large rigid-body domain movements are critical to GroEL-mediated protein folding, especially apical domain elevation and twist associated with the formation of a folding chamber upon binding ATP and co-chaperonin GroES. Here, we have modeled the anisotropic displacements of GroEL domains from various crystallized states, unliganded GroEL, ATPγS-bound, ADP-AlFx/GroES-bound, and ADP/GroES bound, using translation-libration-screw (TLS) analysis. Remarkably, the TLS results show that the inherent motions of unliganded GroEL, a polypeptide-accepting state, are biased along the transition pathway that leads to the folding-active state. In the ADP-AlFx/GroES-bound folding-active state the dynamic modes of the apical domains become reoriented and coupled to the motions of bound GroES. The ADP/GroES complex exhibits these same motions, but they are increased in magnitude, potentially reflecting the decreased stability of the complex after nucleotide hydrolysis. Our results have allowed the visualization of the anisotropic molecular motions that link the static conformations previously observed by X-ray crystallography. Application of the same analyses to other macromolecules where rigid body motions occur may give insight into the large scale dynamics critical for function and thus has the potential to extend our fundamental understanding of molecular machines.

Published by Elsevier Ltd.

Keywords: chaperonin; translation-libration-screw; crystallographic refinement; structural dynamics; protein folding

Introduction

The molecular chaperonin GroEL, along with its co-chaperonin GroES, form a dynamic macromolecular complex that mediates protein folding in the bacterial cell, concurrent with the consumption of ATP.[1] GroEL is made of two heptameric rings that stack back-to-back with dyad symmetry.[2] Non-native polypeptides bind to hydrophobic sites located on the apical domains at the end of the central channel[3–7] (Figure 1(i) and (v)). Folding is initiated by the positive cooperative binding of seven ATP molecules[8–11] followed by the binding of the heptameric co-chaperonin GroES[12] to the same ring (*cis* ring). This generates large, nearly rigid body movement of the intermediate and apical domains of the *cis*-ring subunits that dramatically enlarges and seals the GroEL *cis* cavity. The process of forming this sealed chamber, referred to as the Anfinsen cage, occludes the hydrophobic binding surfaces, thereby releasing the polypeptide into the cavity to initiate folding[13–15] (Figure 1(ii) and (iii)). The GroEL–GroES complex holds the polypeptide for ~ten seconds in a hydrophilically lined cavity.[16–19] Following ATP hydrolysis (Figure 1(iv)), the products of this "half-cycle", ADP and product polypeptide, are released along with GroES, as another similar folding-active assembly is formed in the opposing or *trans* ring[19,20] (Figure 1(v) and (vi)). The behavior of the *trans* ring is 180° out of phase with the *cis* ring, due to the negative cooperativity between the rings.[21,22]

Several conformational states of the GroEL–GroES

Abbreviations used: ADPs, anisotropic displacement parameters; TLS, translation-libration-screw; FOM, figures-of-merit; NCS, non-crystallographic symmetry.

E-mail address of the corresponding author: pdadams@lbl.gov

0022-2836/$ - see front matter Published by Elsevier Ltd.

macromolecular complex have been captured by trapping functionally meaningful intermediates and elucidating their three-dimensional structures. Theoretical studies employing normal mode calculations[23] and targeted molecular dynamics[24] have been used to analyze the transitions that occur during the GroEL cycle. The results suggest that the hinge bending and twisting domain displacements observed in the structures arise from intrinsic flexibility of the subunits. The analyses also give insight into the complex pathway of subunit displacements required for the allosteric transitions in GroEL. However, experimental studies of the dynamical properties of the various structural intermediates in the reaction cycle are necessary to fully understand the basis of the transitions from one state to another.

X-ray crystallography is recognized as one of the most powerful experimental techniques for elucidating the static and the dynamic structure of proteins, since the diffraction data can provide detailed information about atomic displacements in macromolecules. The magnitude and directionality of atomic displacements from the observed X-ray diffraction data can be described using anisotropic displacement parameters (ADPs), which can be interpreted in the light of protein function. Data that extend to atomic resolution (better than 1.2 Å) are required to provide a sufficient observation-to-parameter ratio for the refinement of individual atomic ADPs, since the individual ADP description requires fitting of six independent parameters per atom in the model. However, X-ray atomic displacements are typically dominated by a few low frequency modes correlated over many atoms so that refinement of ADPs for each atom is, in many cases, an over parameterization of the problem. The number of independently fitted parameters can be reduced by assuming a physical model that imposes correlations amongst the ADPs, thus allowing refinement of ADPs against moderate resolution (3–1.5 Å) data. The translation-libration-screw (TLS) method treats groups of atoms as rigid bodies, for which only translations and rotations (librations) about a fixed point are allowed.[25] Each rigid group introduces only 20 independent parameters into the refinement. Displacements of the rigid bodies are fitted to the diffraction data yielding refined TLS tensors that describe the correlated anisotropic displacements of the atoms in each rigid body. Refinement of normal modes, which also describe collective atomic motions, against crystallographic data is a related, but different, approach that has also been used to model atomic displacements.[26] While TLS tensors do not describe the individual normal modes of a molecule, they do approximate the effects of a collection of the low frequency modes.

TLS refinements have been carried out in a number of systems such as bovine ribonuclease A,[27] DLM-1-Z-DNA complex,[28] the LH2 light-harvesting complex,[29] calmodulin,[30] and phospholipase A.[31] Refinement of the light harvesting complex II at 2.0 Å was used to characterize molecular displacements important in optimizing modulation of pigment energy interactions in photosynthetic energy transfer. Calmodulin was refined at atomic resolution (1.0 Å) to study the role of discrete disorder in achieving the structural plasticity required for its physiological role of binding several protein targets in response to a Ca^{2+} signal. Similar approaches have been used to gain insight into internal motion, anisotropy, disorder, and the implications for mechanism in the other systems mentioned above. However, TLS analysis has yet to be used to study rigid-body motions in large macromolecular complexes.

The multi-domain structure of the GroEL–GroES complex and the large domain movements associated with the conformational changes lend themselves to a rigid-body TLS analysis, with the aim of understanding the underlying molecular properties that give rise to the observed structural changes in the activation process. The availability of atomic crystal structures of GroEL, tracking the conformational changes upon binding nucleotide and GroES in the progression of its reaction cycle, and recent improvements in the implementation of TLS refinement methodology makes it possible to extract additional experimental information about the chaperonin reaction cycle. We have increased the information content of the various models of the chaperonin obtained from the diffraction data by modeling anisotropic displacements in order to gain insight into the motions in different functional states. We show that the chaperonin dramatically changes its dynamic properties through the various states, and consider the implications for the functioning of this molecular machine.

Results and Discussion

Common features of TLS refinements

The three-dimensional X-ray crystal structures of the GroE system studied by TLS refinement are: (1) unliganded GroEL[2,32] (Figure 1(i)), (2) GroEL fully complexed with 14 ATPγS molecules[33,34] (Figure 1(ii)), (3) the asymmetric $GroEL_{14}$–$GroES_7$–$(ADP \cdot AlF_x)_7$ complex[15] (Figure 1(iii)) which corresponds to the folding active state, and (4) the post-hydrolysis $GroEL_{14}$–$GroES_7$–ADP_7 complex[14] (Figure 1(iv)). After generating starting models, TLS refinements were performed (see Methods). The TLS parameters were then fixed and residual isotropic *B*-factors were refined. These represent the residual internal motions of the quasi-rigid groups, for example individual side-chains, which cannot be adequately described by the TLS model. Refinements of the same starting models were also performed using isotropic *B*-factor refinement alone (see Methods). In all cases, the inclusion of the TLS parameterization represents an improvement over isotropic *B*-factor refinement alone, lowering the crystallographic free *R*-value

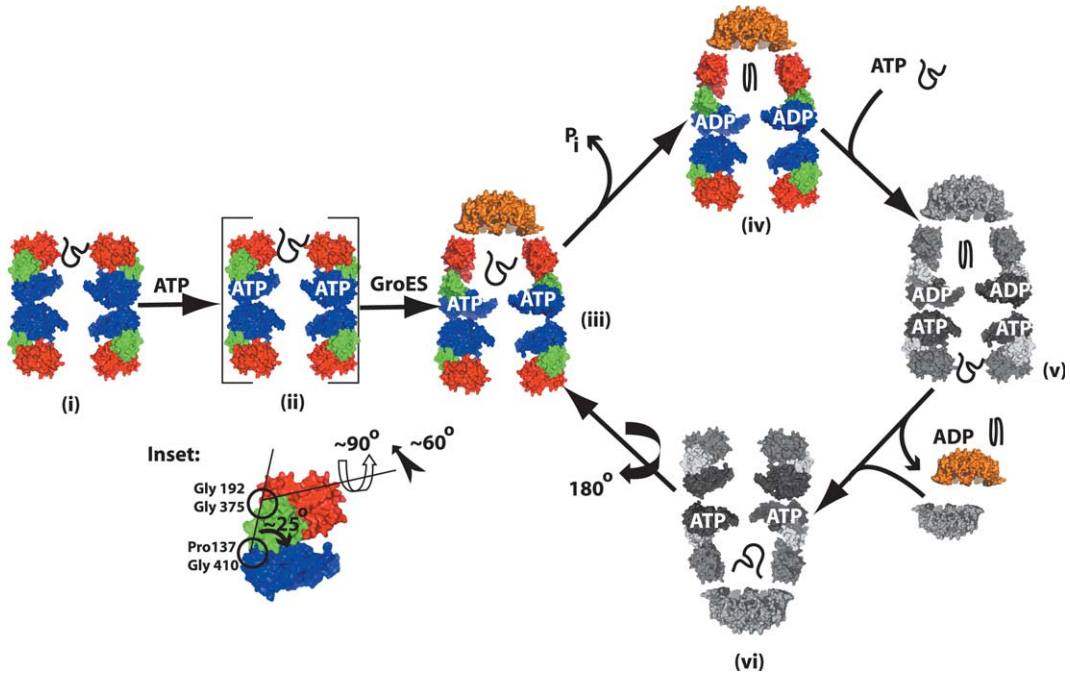

Figure 1. Schematic of the functional states in the GroEL reaction cycle and the underlying domain mechanics. (i) Non-native polypeptide substrate (black line) binds to the hydrophobic apical domains of an open GroEL ring. Inset: the direction and magnitude of the *en bloc* domain movements within an individual subunit of the *cis* GroEL ring accompanying future binding of ATP and GroES are shown. (ii) ATP binding to GroEL results in a conformational change that weakens substrate affinity, and enables GroES binding to the ATP-bound ring. (iii) Binding of GroES induces a large conformational change in GroEL that leads to an approximate doubling of the volume of the central cavity and obscures GroEL's hydrophobic polypeptide recognition regions, releasing the substrate into the encapsulated cavity to fold. ATP bound to the *cis* complex acts as a timer, giving the substrate eight to ten seconds to fold inside the cavity. (iv) Substrate polypeptide folds in the relatively polar environment of the *cis* cavity and ATP is hydrolyzed. This produces a weakened *cis* assembly that is primed for release of GroES. (v) After *cis* hydrolysis, a second non-native polypeptide and ATP bind to the *trans* ring, discharging the *cis* ligands and initiating new GroES binding to the lower ring (vi) to form a new folding active complex. GroEL acts as a "two-stroke-engine" so that the cycle on the lower ring is the same but 180° out of phase with the upper ring. The apical, intermediate, and equatorial domains are red, green, and blue, respectively, while GroES is orange. This coloring scheme is maintained in the subsequent Figures.

(Table 1). The best results were obtained when each of the domains in a GroEL subunit and a GroES subunit were treated as independent rigid bodies, as opposed to whole-ring or whole-subunit TLS models, indicating that the inclusion of relative domain displacements significantly improves the quality of the model. The relatively simple TLS model accounts for the majority of the atomic displacements; hence the residual isotropic *B*-factors are essentially constant (Figure 2(a)). The inclusion of TLS parameters generates an average isotropic *B*-factor distribution that closely matches that from isotropic *B*-factor refinement alone, while permitting greater local variation in ADPs (Figure 2(a)). A comparison of the thermal ellipsoids for a subunit in the unliganded GroEL structure generated from both a restrained isotropic refinement (Figure 2(b)) and a TLS refinement (Figure 2(c)) shows that anisotropy is better modeled in the latter case.

Table 2 lists the magnitudes of both the translational and librational components of the various TLS models for the rigid-body domains. Within each structure, the translational and librational tensor eigenvalues get progressively larger when moving away from the equatorial region, through the intermediate and apical domains, and finally to GroES. However, it is clear from the relative magnitudes of the translational and librational tensor eigenvalues that the motion in all domains is primarily characterized by libration. Analysis of the motion reveals that the librations of the individual domains have different magnitudes and directions, underscoring that there are complex composite motions of the domains connected by the hinges in the GroEL–GroES machine. We focus mainly on the libration axes in the analysis that follows, considering the distinct character of the librational motion of the various domains within each structure.

Inherent motion of GroEL in a polypeptide acceptor state

Displacements of individual domains

The principal axes of the libration tensors for the three domains in the unliganded GroEL subunit are shown in Figure 3. There are two primary librations within the equatorial domain, both in the plane

Table 1. Crystallographic data and refinement statistics

	GroEL	GroEL–ATPγS	GroEL–GroES–ADP·AlF_x	GroEL–GroES–ADP
Diffraction data				
Resolution (Å)	30.0–2.70	40.0–2.0	50.0–2.8	50.0–3.0
Space group	$C222_1$	$P2_1$	$P2_12_12$	$P2_12_12$
Unit cell parameters (Å)	$a=178.38$, $b=204.98$, $c=280.98$, $\alpha=\beta=\gamma=90°$	$a=135.57$, $b=260.11$, $c=150.20$, $\alpha=\gamma=90°$ $\beta=101.14°$	$a=255.55$, $b=266.86$, $c=187.05$, $\alpha=\beta=\gamma=90°$	$a=255.26$, $b=265.25$, $c=184.40$, $\alpha=\beta=\gamma=90°$
Molecules per asymmetric unit	1	1	1	1
Unique reflections	114,859	530,143	231,127	229,816
Redundancy	Not available	2.6 (not available)	4.0 (3.2)	3.3 (2.4)
Completeness (%)	88.2 (53.6)	97.8 (95.7)	90.3 (55.0)	96.7 (91.2)
$I/\sigma(I)$	12.4 (1.6)	10.2 (1.5)	6.6 (1.3)	9.1 (1.8)
R_{sym} (%)	Not available	9.6 (78.1)	13.8 (60.1)	12.1 (53.0)
Model statistics				
Data range (Å)	30.0–2.70	40.0–2.0	50.0–2.8	50.0–3.0
$R_{cryst,\ best\ isotropic\ model}$ (%)	22.2 (34.0)	25.8 (45.0)	26.4 (46.0)	27.2 (36.0)
$R_{free,\ best\ isotropic\ model}$ (%)	25.7(36.0)	27.6(49.0)	28.8 (53.0)	30.2 (42.0)
$R_{cryst,\ TLS\ model}$ (%)	21.5 (33.0)	24.5 (46.0)	24.7 (43.0)	25.7 (35.0)
$R_{free,\ TLS\ model}$ (%)	24.9 (37.0)	26.5 (47.0)	27.4 (52.0)	28.7 (38.0)
Number of protein atoms	26,957	53,984	59,276	59,276
Number of TLS groups	21	42	49	49
Number of adenine molecules	0	14	7	7
Number of AlF_x molecules	0	0	7	0
Number of Mg^{2+} atoms	0	14	7	7
Number of K^+ atoms	0	16	7	7
Number of solvent atoms	117	956	211	187
Mean bond-length deviation (Å)	0.027	0.026	0.027	0.024
Mean angle deviation (deg.)	2.043	1.961	2.039	2.034
Residues in core ϕ–ψ region (%)	91.7	91.0	89.6	88.2
Residues in disallowed regions (%)	0.0	0.0	0.0	0.0

$R_{sym} = \sum |I_h - \langle I_h \rangle| / \sum I_h$, where $\langle I_h \rangle$ is the average over Friedel and symmetry equivalents. $R_{cryst} = \sum ||F_o| - |F_c|| / \sum |F_o|$, where F_c is the calculated structure factor. R_{free} is as R factor but calculated for 2% of randomly chosen reflections that were omitted from the refinement. Values reported in parentheses are for the last shell.

normal to the cylindrical 7-fold axis. The largest libration axis (E1) is tangential to the ring of equatorial domains, while the other axis points into the center of the ring (not shown). By contrast, libration about the third axis (not shown) parallel with the central 7-fold is almost negligible. Librations about the two primary axes result in displacements of the equatorial domain that produce tilting and rocking motions in the plane normal to the cylindrical 7-fold axis. These would allow the domains the required flexibility for changes in tilt that occur in the transmission of negative cooperativity across the rings.

The intermediate domain, which links the equatorial domain to the apical domain and as such is a major component of allosteric communication in GroEL, has two primary librations (Figure 3). Rotation of the intermediate domain about its predominant libration axis I1 results in a combined up–down and side-to-side twisting motion about the lower hinge (Figure 4). As a result of this motion the upper hinge of the intermediate domain is pulled in and out with respect to the central cylindrical axis, leading to raising/lowering and twisting of the covalently attached apical domain. Such opening and closing motions of the apical domain may have a role in polypeptide capture and binding. Displacements about the second libration axis I2 result in an up and down motion of the intermediate domain about the lower hinge, an extreme downward extent of which would move the intermediate domain to cover the ATP-binding site of the equatorial domain.

The apical domain is the least-resolved of all the domains in the GroEL molecule with high *B*-factors and conformational variability,[32] suggesting an intrinsic flexibility that may be functionally necessary to accommodate binding of structurally diverse target polypeptides in the central channel. Consistent with this, the TLS results reveal that the apical domain undergoes extensive librations about three orthogonal axes (Figure 3). The apical domain motion is thus inherently isotropic, suggesting that it is the directed movement of the intermediate domain that drives the opening and closing of the central cavity (Figure 4). Supporting this is the observation that in the GroEL–ATPγS crystal structure[34] both the intermediate and apical domains are displaced as a single rigid body when compared with unliganded GroEL (not shown). The success of the TLS refinement in modeling the atomic displacements throughout the GroEL molecule suggests that the primary motion of the apical domain is as a rigid-body.

Inherent motions in GroEL reflect the path taken on binding ATP and GroES

Examination of the directions of the libration axes of the intermediate and apical domains within the unliganded GroEL subunit reveal displacements that are directly related to the structural changes that will occur when ATP (simulated with a transition state analog of ATP hydrolysis, $ADP \cdot AlF_x$) and GroES bind converting the chaperonin into its *cis* folding-active state. Therefore, they are predictive of the motions the domains will undergo in future states along the reaction coordinate.

In transitioning from the polypeptide-binding to folding-active state there is motion of the intermediate domain around the lower hinge-point, and motion of the apical domain around the upper hinge point (Figure 1, inset). To understand the relationship between these domain motions and our TLS results, we tested possible rotations about the TLS libration axes. A downward motion of the intermediate domain is generated by a rotation about principal TLS libration axis I1 (Figure 5(a)), combined with a rotation about the second libration axis I2 (Figure 5(b)). In combination, these two rotations bring the unliganded intermediate domain closer to the equatorial domain, as in the folding-active state. An upward motion of the apical domain is generated by a rotation about TLS libration axis A1 (Figure 5(c)), combined with a rotation about libration axis A2 (Figure 5(d)). These two rotations move the apical domain to a raised open conformation similar to that observed in the folding-active state. Rotation around the third libration axis, A3 (Figure 3) appears to be negligible but may be a necessary component of the conformational transition pathway from the polypeptide binding to the final folding-active state.

We conclude that the observed atomic displacements in the GroEL molecule are not random in nature but instead are directed along the same transition pathways that, in the presence of ATP and GroES, lead to the *cis* folding-active conformation. It should be noted, however, that the magnitudes of the TLS librations do not predict the magnitude of the observed ligand-driven displacements. The absolute values could be governed by transient interactions in the conformational transition and limitations imposed by the crystalline environment. Our results do suggest, however, that the observed anisotropic molecular motions are consistent with large-scale movements that occur in solution[35] (F. Motojima & A.H., unpublished observations).

Inherent motion of the GroES-bound GroEL subunit

How do the dynamic properties of the domains change once ATP and GroES are bound? Analysis of the libration tensors in the *cis* GroEL subunit (Figure 6) indicates that they are significantly changed in direction and magnitude compared to unliganded GroEL. The most striking changes in dynamical properties occur in the substrate binding apical domains. The TLS results indicate that the apical domain now has a highly anisotropic in-place rotation which is roughly aligned with the central 7-fold, in contrast to the isotropic motion observed in unliganded GroEL (compare Figure 6 with Figure 3).

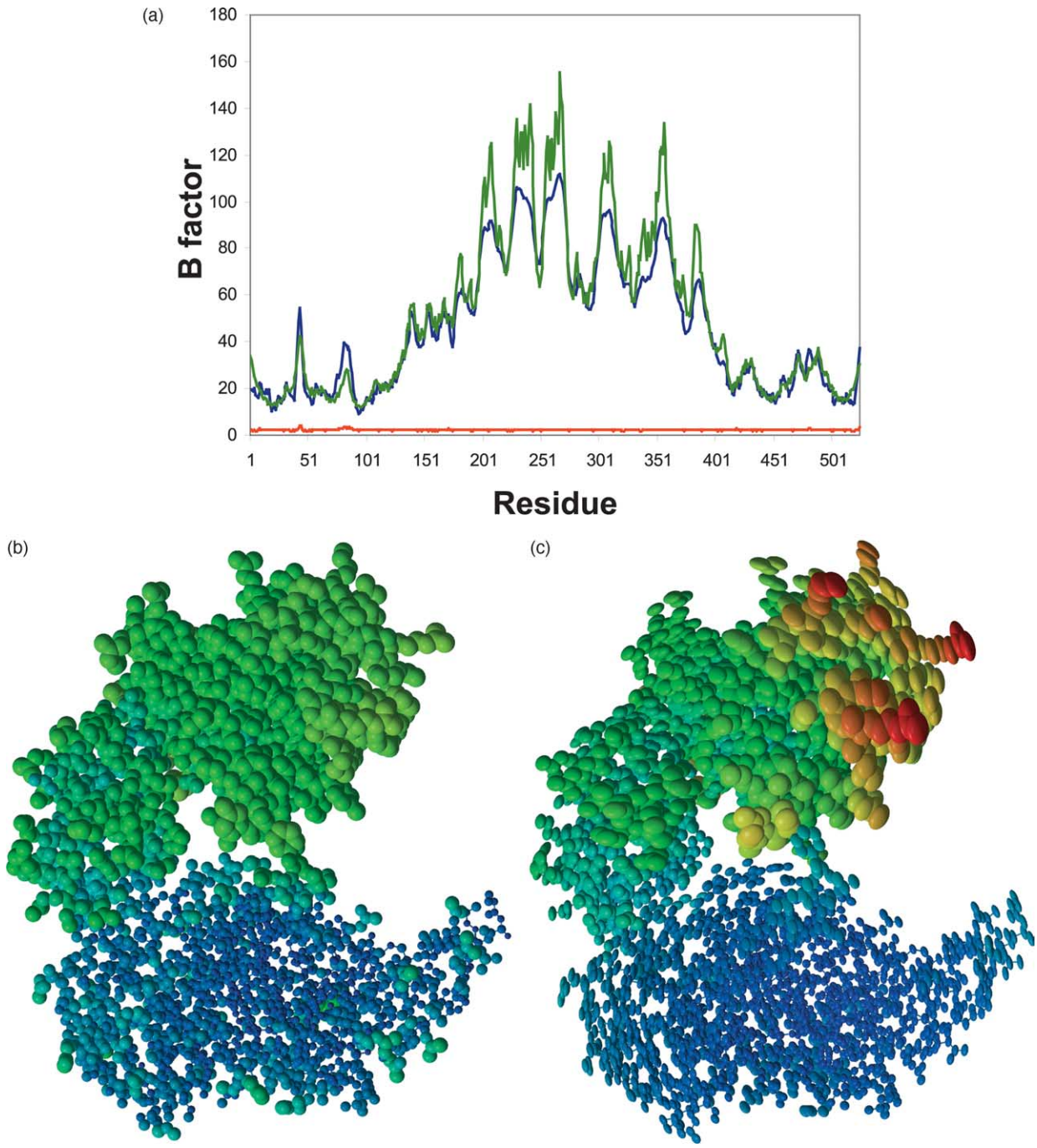

Figure 2. Improved modeling of anisotropy with TLS refinement. (a) A comparison of residue-averaged isotropic *B*-factors of a representative unliganded GroEL subunit from both a restrained isotropic refinement in REFMAC (blue line) and a TLS refinement in REFMAC (green line), where $\langle B_{iso} \rangle$ is the equivalent isotropic *B*-factor calculated as the trace of each atomic U_{ij}; atomic anisotropic U_{ij} parameters are derived from the decomposition of the TLS tensors using the TLSANL program. The residual $\langle B_{iso} \rangle$ after TLS refinement (red line) is negligible. (b) and (c) Atomic displacement parameters (ADPs) for an unliganded GroEL subunit calculated from both the TLS model (c) and the isotropic model (b) are shown colored according to the magnitude of the displacements, ranging from blue (smallest) to red (largest).

In this folding-active conformation a salt-bridge interaction between residues in the apical domain (Arg197) and the neighboring subunit's intermediate domain (Glu386) is broken. The apical domain then elevates and twists to form new interfaces with neighboring apical domains and GroES, which binds as a lid to the collective of apical domains, capturing and stabilizing them in their new elevated conformation (Figure 9(a) and (b)). The binding results in a strong coupling between GroES and the apical domains, which is reflected in the shared directions and magnitudes of their predominant motions (Figure 8(a)).

The intermediate domain now has three libration axes (Figure 6). Its dynamic character is dominated by motion about the largest libration axis I1. A

Table 2. TLS tensor eigenvalues for the GroE structures

	GroEL		GroEL–ATPγS		GroEL–GroES–ADP·AlF$_x$		GroEL–GroES–ADP	
Residues in TLS groups	Libration (deg^2)	Translation (Å^2)	Libration (deg^2)	Translation (Å^2)	Libration (deg^2)	Translation (Å^2)	Libration (deg^2)	Translation (Å^2)
GroES (1–97)								
Mean	–	–	–	–	7.96	1.69	12.06	1.07
σ	–	–	–	–	1.01	0.04	0.88	0.05
Anisotropy	–	–	–	–	1.57	1.69	1.73	2.58
Apical domain of *cis* ring (191–374)								
Mean	8.38	0.62	13.17	0.54	8.74	1.71	10.70	1.48
σ	0.74	0.11	5.57	0.14	1.67	0.16	1.32	0.16
Anisotropy	1.70	1.41	1.65	1.64	3.91	1.59	3.36	1.80
Intermediate domain of *cis* ring (136–190, 375–409)								
Mean	5.55	0.37	9.23	0.33	6.44	0.67	5.90	0.58
σ	0.84	0.09	3.25	0.11	0.44	0.14	0.66	0.15
Anisotropy	8.39	1.30	2.59	1.04	2.65	1.97	2.30	1.79
Equatorial domain of *cis* ring (2–135, 410–525)								
Mean	1.84	0.12	1.90	0.08	2.87	0.41	2.24	0.27
σ	0.19	0.02	0.56	0.04	0.31	0.09	0.18	0.08
Anisotropy	3.15	5.48	3.95	3.27	9.78	1.50	7.04	1.07
Equatorial domain of *trans* ring (2–135, 410–525)								
Mean	–	–	1.70	0.13	3.93	0.38	3.55	0.25
σ	–	–	1.00	0.02	0.27	0.08	0.33	0.06
Anisotropy	–	–	4.42	1.81	6.77	1.23	6.12	1.38
Intermediate domain of *trans* ring (136–190, 375–409)								
Mean	–	–	10.26	0.44	6.21	0.83	5.90	0.73
σ	–	–	5.69	0.04	1.32	0.14	1.15	0.18
Anisotropy	–	–	3.66	1.50	3.12	7.84	1.83	1.59
Apical domain of *trans* ring (191–374)								
Mean	–	–	13.60	0.56	7.35	1.23	8.10	1.00
σ	–	–	8.44	0.09	0.59	0.17	0.30	0.13
Anisotropy	–	–	1.04	1.28	1.73	1.07	2.02	2.21

Mean values of libration and translation tensors are derived by averaging the trace of each tensor for all the NCS copies of a TLS group. σ is the standard deviation from the mean. Anisotropy is $|\mathbf{P}_{max}|/|\mathbf{P}_{min}|$, where $\mathbf{P}_{max}$ is the largest ellipsoid axis and $\mathbf{P}_{min}$ is the smallest, and defines the degree of distortion from a sphere.

result of this motion is a tilting of the intermediate domain into and out of the central cavity (Figure 7), which should be contrasted with the motion of the intermediate domain in the unliganded GroEL subunit (compare to Figure 4). This is the result of increased coupling between intermediate and equatorial domains in the *cis* GroEL assembly, where there are many interactions between the intermediate domain and the bound nucleotide and equatorial domain, both within the same subunit and with a neighboring subunit.[14,15] Furthermore, minimal coupling between the intermediate and apical domains is now observed due to loss of the intersubunit salt-bridge between the intermediate domain (Glu386) and the apical domain (Arg197) which served to couple the two domains in unliganded GroEL. This switching of intermediate domain coupling underscores that it is a key controlling element in the conformational transition required for GroEL function.

TLS model of GroEL–ATPγS[14]

In a further analysis, we sought to examine the effect of ATP alone on the dynamics of GroEL. The resultant TLS model, compared with that of unliganded GroEL, reveals an increase in the magnitude of the mean librational motion for both the apical and intermediate domains (Table 2), consistent with the notion that the binding of ATP, by mobilizing the intermediate and apical domains, initiates the structural transition that enables GroES binding. Notably, our results are in agreement with conclusions from an independent normal mode analysis of an unliganded and ATPγS bound GroEL subunit that suggest that the intermediate and apical domains become more flexible upon ATP binding as compared with the unliganded GroEL subunit.[23]

TLS model of GroEL–GroES–ADP$_7$

What changes occur in the dynamic properties of the *cis* chamber upon hydrolysis? The most striking difference in the TLS model for the GroEL–GroES–ADP·ALF$_x$ and ADP structures resides in the libration motion for the apical domains and GroES. The predominant libration axes in both GroES (ES1) and the apical domains (A1) are larger in the post-hydrolysis ADP complex as compared with the ADP·ALF$_x$ complex (compare Figure 8(b) with Figure 8(a)). In addition, the spread of the axes between NCS related copies for both GroES and the apical domain is also larger in the ADP structure (not shown). Together, the increased magnitude and angular spread of these librational axes indicates an

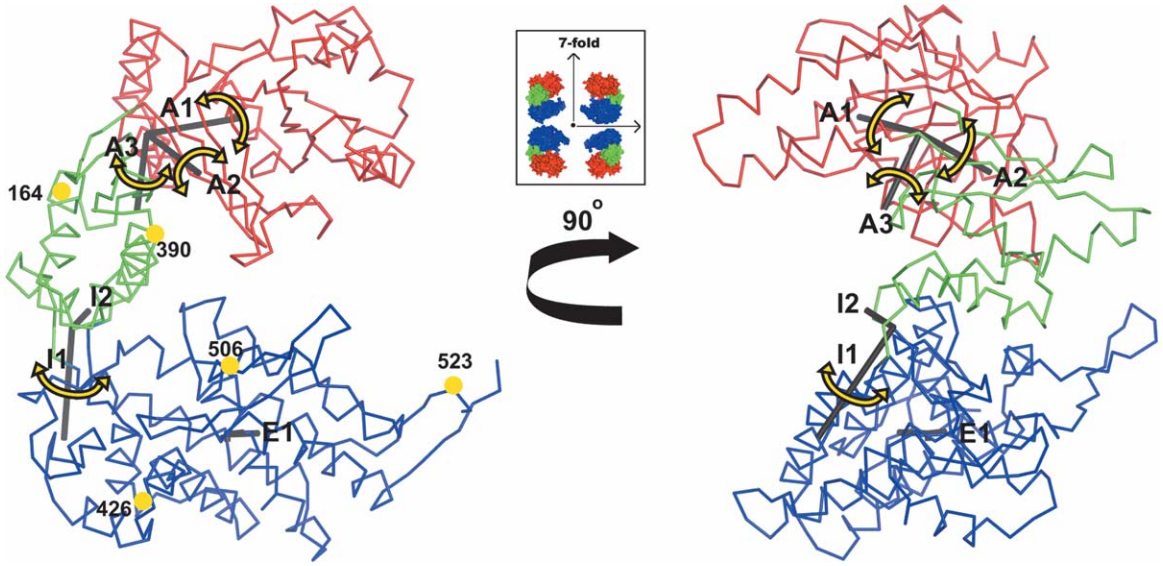

Figure 3. Principal axes of the libration tensors for the three domains of the unliganded GroEL subunit in the polypeptide-binding state. Two orthogonal views of a C^{α} trace of a representative subunit are shown. Views are perpendicular to the 7-fold, which is aligned vertically in the plane of the page. The inset shows three orthogonal reference axes corresponding to the central 7-fold rotation axis, an axis from the ring center coming out of the page, and a third orthogonal axis parallel with a ring tangent. For each domain, the principal axes displayed represent the mean of the distribution for all seven NCS related domains. Axes are labeled in ascending order, from the largest libration to the smallest. The primary librations are indicated with rotational arrows. Yellow colored circles denote residues in this standard subunit view that are useful for visual orientation in Figure 5.

increased rotational motion of GroES on GroEL in the post-hydrolysis weakened *cis* complex. We interpret these changes as a reflection of increased mobility of GroES and the apical domains in the ADP state, which arise from the less stable interaction observed biochemically between them.[15,19] The large rotational displacements of GroES approximately parallel with the GroEL cylindrical axis may have implications for how GroES departs from the ADP cavity, i.e. by a twisting off motion.

Positive cooperativity and intra-ring interactions

Can information about cooperativity in the structural transition from the unliganded to GroES-bound state be extracted from the TLS analyses? The libration tensors in unliganded GroEL indicate the directions of movements the domains undertake in the transition, involving a downward motion of the intermediate towards the equatorial domain and an upward rotation of the apical domain. These movements can only be accommodated in the heptameric ring if they are concerted. Consistent with this, a previous targeted molecular dynamics study following the trajectory of the conformational transition of a GroEL subunit suggests that the basis of the intra-ring positive cooperativity in GroEL lies in (i) steric clashes that arise if one subunit changes conformation and its neighbor does not; and (ii) breaking of the inter-subunit Arg197-Glu386 salt-bridge due to the downward movement of the intermediate domain and the upward movement of the apical domain.[24]

The atomic displacement parameters derived from the TLS refinements can be probed to determine the correlated motions between different regions of the structure. The prediction of the allosteric model is a disappearance of correlation between residues in the vicinity of the salt-bridge and an appearance of correlation between the secondary structural elements that stabilize the *cis* GroES-bound conformation. The positions of these structural elements within a subunit in both GroEL and the ADP·AlF_x *cis* complex are shown for reference in Figure 9(a) and (b). These include residues in the vicinity of the Arg197-Glu386 salt-bridge and the secondary structural elements that contribute to the coupled conformational transition and form the new interface between equatorial and intermediate domains (helix C of one subunit, helix M and the stem-loop of a neighboring right subunit). A Rosenfeld analysis[36] was used to examine the anisotropic displacement parameters of these particular regions. This analysis determines the difference in the projection of the atomic displacement parameters of a pair of atoms along the line joining the centers of the two atoms. While small difference values indicate that the two atoms display a high degree of correlation in the direction and magnitude of their displacements, large difference values indicate that the two atoms are not coupled. It should be noted that we are examining secondary structures from different TLS rigid groups, and therefore high correlations are not a result of the TLS restraints imposed by the rigid-body definition. Figure 10(a) shows the Rosenfeld matrices for residues in the vicinity of the salt-bridge

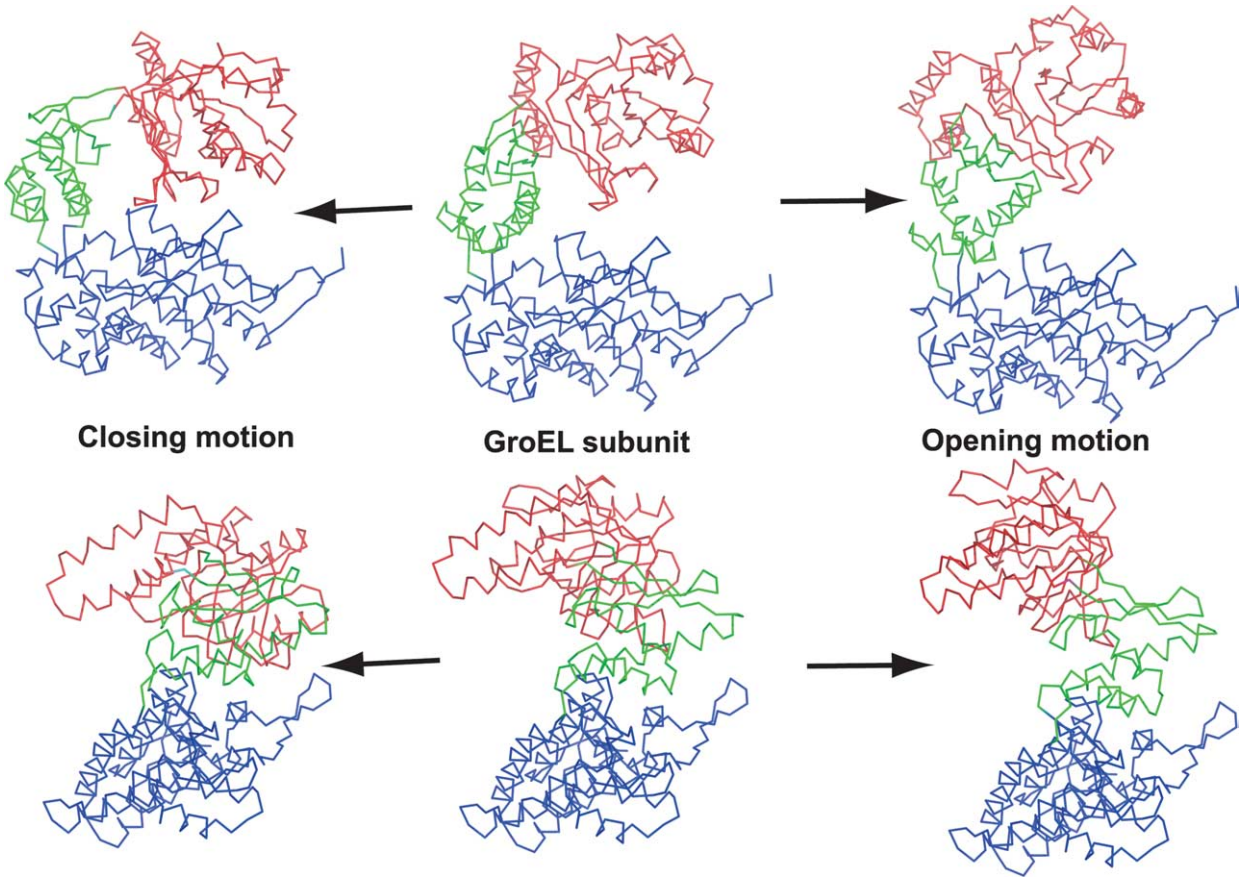

Figure 4. Effect of intermediate domain motion on apical domain in unliganded GroEL. For illustrative purposes, we have performed 25° clockwise and 25° counterclockwise rotations about the predominant libration axis of the intermediate domain (I1, see Figure 3). Two orthogonal views (top and bottom) of the resultant coordinates, related by a 90° vertical rotation are shown to capture the complex motion. The top views are looking approximately from a neighboring subunit in the ring, while the bottom views are from outside the ring looking towards the central 7-fold axis.

in both unliganded GroEL (left) and GroEL–GroES–ADP·AlF_x (right). While there are regions of high correlation in the GroEL structure, these disappear in the AlF_x structure, as predicted from the model. Figure 10(b) shows the Rosenfeld matrices for helix C of one subunit and helix M and the stem-loop for a neighboring subunit in both unliganded GroEL (left) and GroEL–GroES–ADP·AlF_x (right). In this case, there are several regions of elevated difference values in the GroEL structure that disappear in the GroES–ADP·AlF_x structure. The thermal ellipsoids describing the anisotropic displacement parameters for these structural elements (Figure 9(c) and (d)) allow a qualitative view of these results.

Conclusions

Here, we carried out TLS refinements of crystal structures corresponding to key states of the GroEL–GroES macromolecular machine in order to probe the underlying structural dynamics operating during the protein folding cycle. These analyses have captured essential aspects of the movements in the reaction cycle, providing the first experimentally derived view of the dynamics of the GroEL machine. Our results indicate that binding of nucleotide and GroES causes large changes in the dynamic properties of the individual GroEL domains in the progression of the reaction cycle. Furthermore, we could follow the route by which the conformational change is passed onward around the GroEL ring by using correlations in TLS-derived atomic displacement parameters to monitor the changing pattern of structural interactions that coordinate the binding of nucleotide and GroES in the allosteric transition from polypeptide-binding to folding-active states. Within the fairly well resolved set of major states of the machine, the TLS results have enabled predictions of the kinds of motions leading from one state to another; i.e. the polypeptide-binding to folding-active states. There are still other states and structural transitions in the machine that have not yet been captured for which the TLS analyses may also be informative. For example, little is understood about the structural changes and allosteric signals involved in GroES departure. We speculate from our TLS results that GroES may leave by a twisting-off motion. Beyond the machine itself, much less is known about the interaction with substrate polypeptides, how their conformations

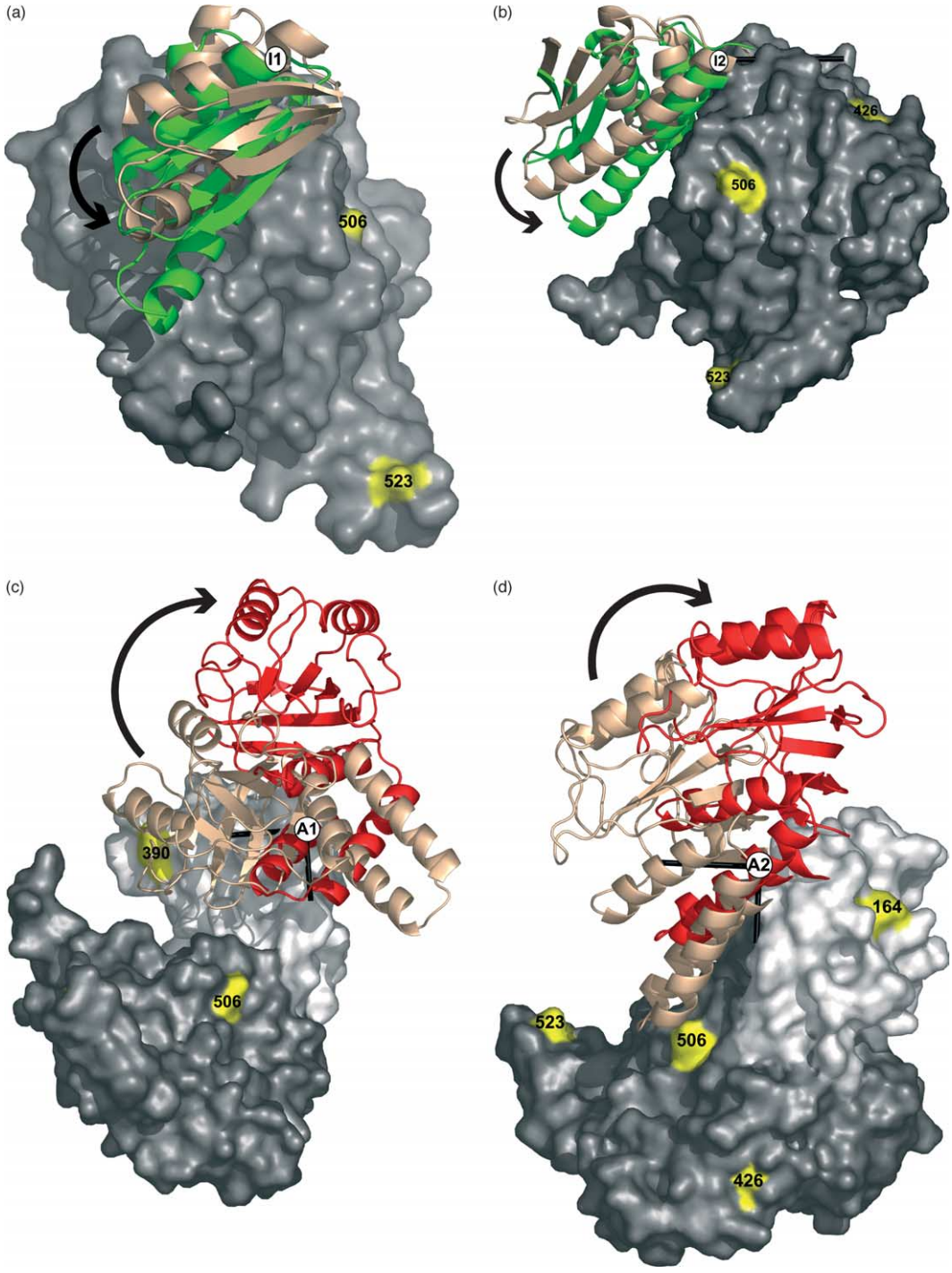

Figure 5. Inherent motions in intermediate and apical domains in unliganded GroEL are already on the path of the structural excursions generated by ATP/GroES binding. To visualize the relationship between the domain motions and the TLS results, possible rotations about the libration axes were tested. (a) and (b) Views are looking down the two major libration axes I1 and I2 of the intermediate domains in GroEL. Intermediate domains in GroEL (wheat) and GroEL–GroES–ADP·AlF_x (green) are shown after least-squares superposition of the two structures using the equatorial domain (gray solvent accessible surface). Rotation of ~30° about I1 relates the intermediate domain coordinates in GroEL with the AlF_x structure (a). After correcting for this rotation, the other predominant transformation comes from a ~20° motion onto the equatorial domain about I2 (b). (c) and (d) Views are looking down two relevant libration axes, A1 and A2, of the apical domains in GroEL. Apical domain in GroEL (wheat) and GroEL–GroES–ADP·AlF_x (red) are shown after least-squares superposition of the two structures using the intermediate domain (white solvent accessible surface). A principle rotation of ~65° about A1 relates the apical domain coordinates in GroEL with the AlF_x structure (c). After subtracting out the changes in coordinates from this first axis, an additional rotation of ~30° is required about A2 to achieve the final position of the apical domain in the AlF_x structure (d). Residues labeled on yellow patches are marked to aid in visual orientation of the subunit with respect to a standard view as a reference shown in Figure 3.

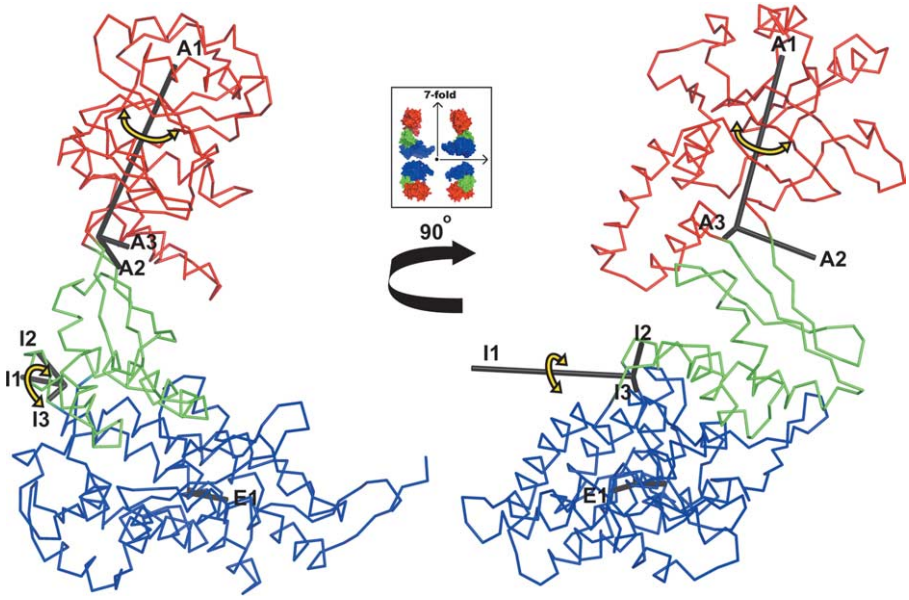

Figure 6. Principal axes of the libration tensors for the three domains in the *cis* GroEL subunit in its folding-active state. Two orthogonal views of a C^{α} trace of a representative subunit in the *cis* (GroES-bound) ring of the GroEL–GroES–ADP·ALF_x complex are shown. For simplicity, librational tensors in the *trans* ring are not shown since they closely resemble those of unliganded GroEL (see Table 2 for magnitudes). Views are perpendicular to the 7-fold, which is aligned vertically in the plane of the page. The inset shows three orthogonal reference axes corresponding to the central 7-fold rotation axis, an axis from the ring center coming out of the page, and a third orthogonal axis parallel with a ring tangent. For each domain, the principal axes displayed represent the mean of the distribution for all seven NCS related rigid body domains. Axes are labeled in ascending order, from the largest libration to the smallest, and therefore axes labels are not equivalent with those in Figure 3. The primary librations are indicated with rotational arrows.

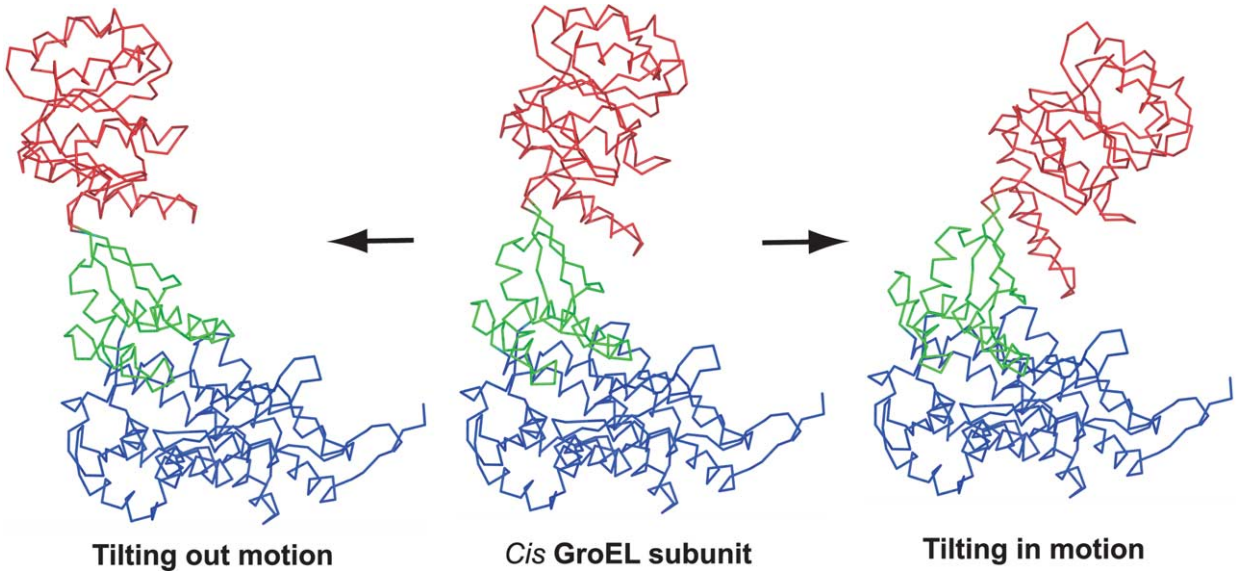

Figure 7. Intermediate domain motion in the *cis* GroEL subunit leads to increased coupling with the equatorial domain. For illustrative purpose, we have performed 25° clockwise and 25° counterclockwise rotations about the predominant libration axis of the intermediate domain (I1, see Figure 6).

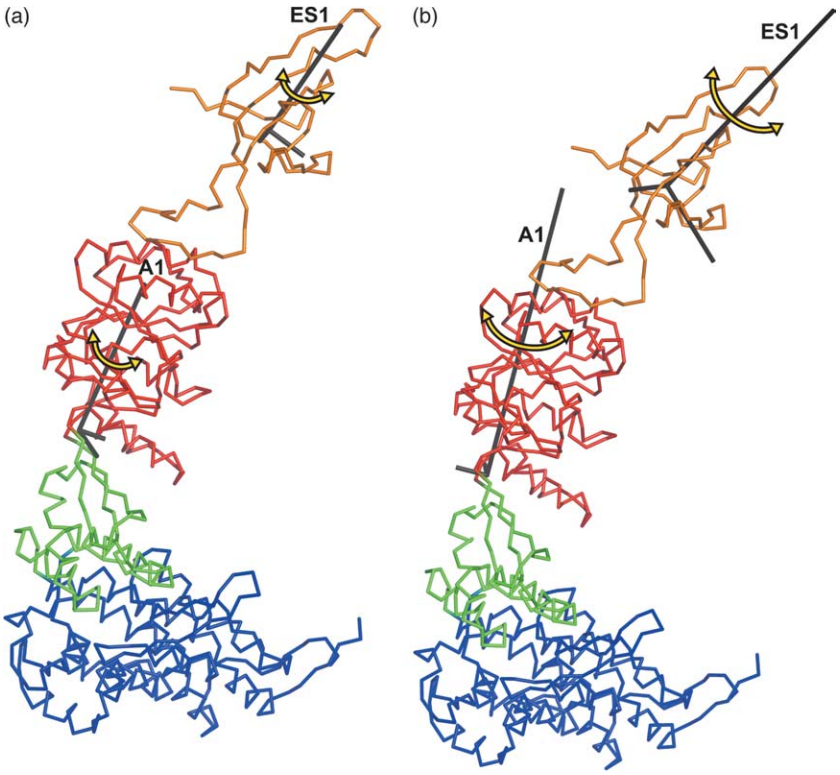

Figure 8. Principal axes of the libration tensors for GroES and the apical domain in *cis* ATP and ADP states. A C^{α} trace of a subunit in the GroES-bound ring of both the ADP·ALF$_x$ (a) and ADP *cis* complex (b) are shown. In both (a) and (b), the principal axes displayed represent the mean of the distribution for all seven NCS related rigid body domains. The apical, intermediate, and equatorial domains are colored as in Figure 3 and GroES is orange.

are affected during the reaction cycle, and how they may affect the machine. It would be revealing for example to study the effects of polypeptide on the dynamics of GroEL. Even though it is unlikely that the disordered polypeptide can be resolved in a crystallographic experiment, the effects on the dynamics of the rest of the system could be studied by TLS analysis.

The success of the TLS model reinforces the idea that domain motions in GroEL are predominantly rigid-body in character. However, with the TLS analysis it is not possible to obtain the timescale of these motions, although the low-frequency modes observable are generally in the multi-picosecond range.[26,37] Other approaches involving time-resolved spectroscopic methods and single-molecule experiments may provide a better experimental window to extract the relevant time scales governing the dynamics of the conformational transitions. Correlating the timescale of the macromolecular motions of the GroEL machine in solution with the events in the chaperonin cycle would extend our present model. Recent advances in both NMR spectroscopy[38] and FRET techniques[39] and their successful application to the chaperonin system may prove valuable in this regard.

Our current study demonstrates a general approach that can be applied to the structural transitions of any macromolecular assembly where large rigid body motions are involved. This has the potential to considerably increase our understanding of complex macromolecular machines that carry out many essential functions in the cell. In the case of GroEL the inherent dynamic modes are indicative of the required conformational changes in the reaction pathway, suggesting that the structure has evolved rigid body motions that facilitate the conformational changes required for function. This may be a fundamental property of molecular motion in macromolecular machines, which has arisen by the natural selection of physical and dynamic properties to optimize function.

Methods

Starting models and diffraction data

Models were obtained from the Protein Data Bank:[40] GroEL (PDB accession code 1OEL), GroEL–ATPγS (PDB accession code 1KP8), GroEL–GroES–ADP (PDB accession code 1PF9), and GroEL–GroES–ADP·AlF$_x$ (PDB accession code 1PCQ). Structure factor amplitudes, experimental error estimates, and cross-validation information were obtained from the PDB for GroEL–ATPγS, GroEL–GroES–ADP, and GroEL–GroES–ADP·AlF$_x$. The corresponding data for GroEL, including experimental phases, were available from previous studies.[2,32]

Calculation of minimally biased electron density maps

A protocol, similar to others described in the literature,[33] was applied to each structure in order to create minimally biased electron density maps for validation of the atomic model. First, a mask was calculated around a representative protomer in the asymmetric unit (chain A in the case of GroEL and GroEL–ATPγS; chains A, H and O in the case of GroEL–GroES–ADP and GroEL–GroES–ADP·AlF$_x$). The mask was expanded and smoothed using the MAMA program.[41] Non-crystallographic symmetry (NCS) operators were calculated from the atomic coordinates. Random phases were then calculated for

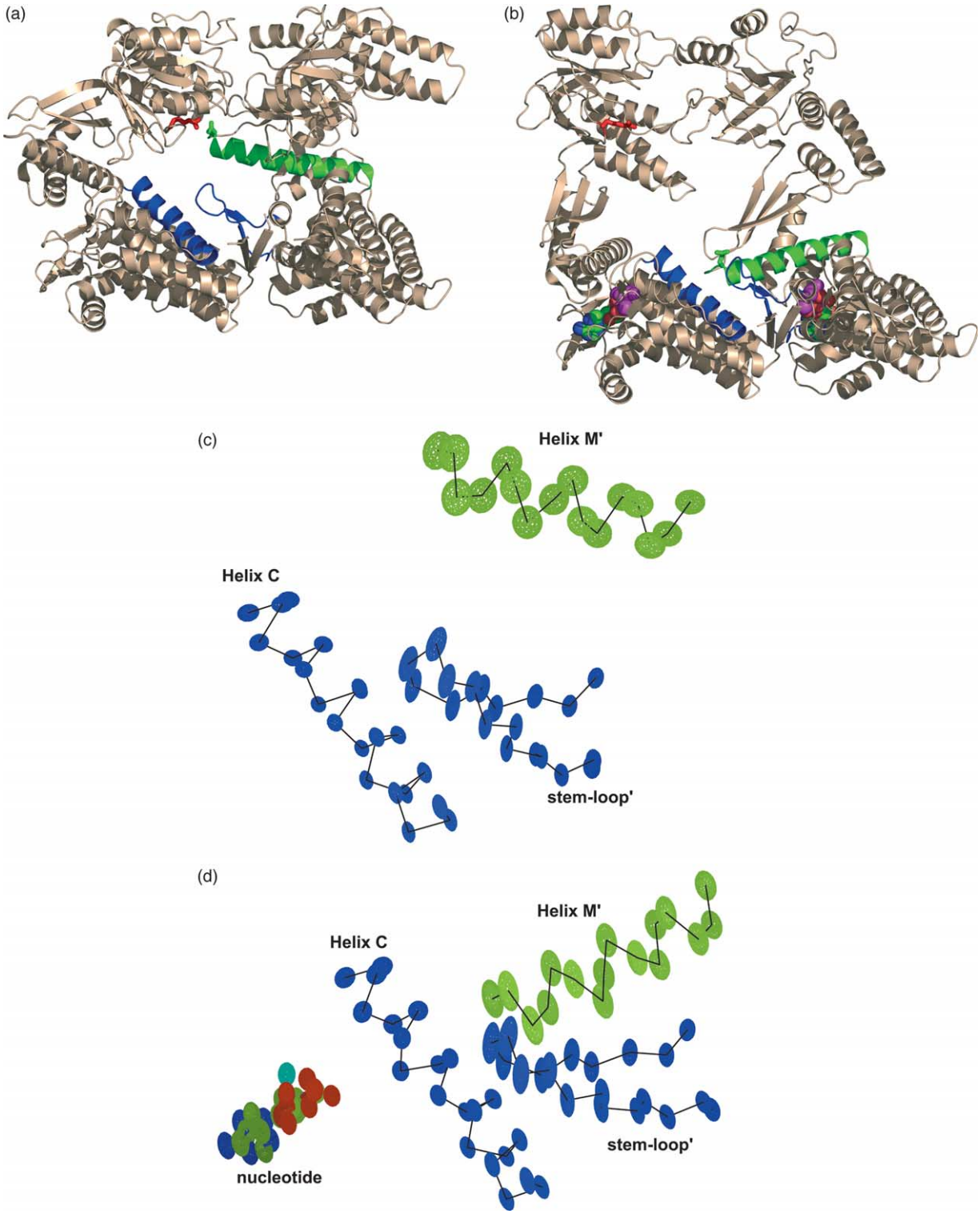

Figure 9. Positive intra-ring cooperativity ((a) and (b)). Substructures of GroEL involved in the cooperative structural transition that leads to formation of the *cis* folding-active complex. Two adjacent subunits are shown for comparison from unliganded GroEL (a) and GroEL–GroES–ADP·AlF_x (b). Helix C in the equatorial domain of one subunit is shown in blue, the stem-loop in the equatorial domain and helix M in the intermediate domain of a neighboring subunit are shown in cyan and green, respectively. Side-chains of Arg197 in the apical domain of one subunit and Glu386 in the intermediate domain of a neighboring subunit are shown in red and green, respectively. (c) and (d) Thermal ellipsoids calculated from the ADPs are shown for helix C of one subunit and helix M and the stem-loop of a subunit in both GroEL (c) and GroEL–GroES–ADP·AlF_x (d).

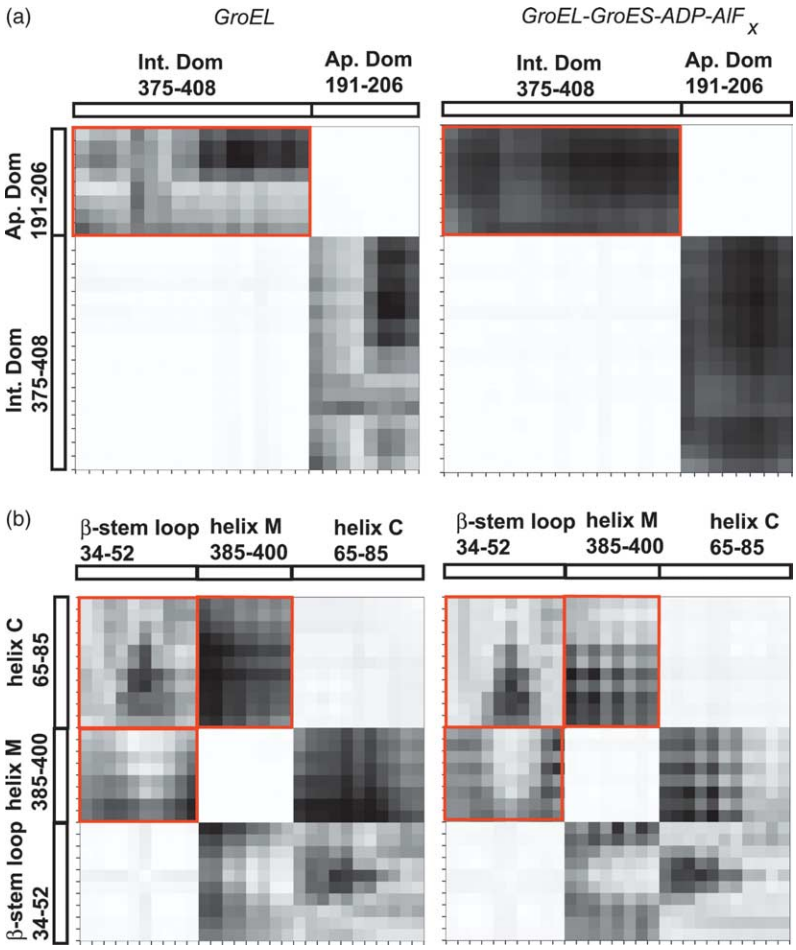

Figure 10. Rosenfeld analysis. (a) Rosenfeld matrices for the ADPs in GroEL (left) and GroEL–GroES–ADP·AlF_x (right) are shown for residues in the proximity of Arg197 in one subunit and Glu386 in a neighbor subunit. (b) Rosenfeld matrices for the ADPs in GroEL (left) and GroEL–GroES–ADP·AlF_x (right) are shown for helix C of one subunit and helix M and the stem-loop of a neighbor subunit. The difference values for ADPs are displayed, with larger differences corresponding to darker boxes. For clarity, the difference values are averaged in bins of two residues.

each experimental observation and figures-of-merit (FOM) were all assigned a constant value of 0.1. The experimental amplitudes, random phases and FOMs were then used as input to density modification in CNS version 1.1.[42] The density modification procedure used the protomer mask and NCS operators to average the electron density. The protomer mask was also used to define the solvent region for solvent flipping.[43,44] The initial resolution limits for the density modification extended from the lowest limit of the experimental data up to 10 Å. This upper resolution limit was slowly extended to the high resolution limit of the experimental data over the course of 200 density modification steps. The improved phases after density modification were used to calculate electron density maps for subsequent visual inspection.

Validation and modification of models prior to refinement

The starting models obtained from the PDB were compared to the minimally biased electron density maps. In all cases a good fit was seen between the coordinates and the density in the equatorial and intermediate domains. However, some differences were observed in the apical domain region for GroEL, GroEL–GroES–ADP and GroEL–GroES–ADP·AlF_x. Therefore, the apical domains in these structures were replaced with the coordinates from the highest resolution GroEL–ATPγS model, which showed a good fit to the minimally biased density. In all cases the remodeled apical domains showed an improved fit to the density. The lack of a high-resolution structure for GroES excluded the possibility of any remodeling. The electron density for this region in the GroEL–GroES–ADP and GroEL–GroES–ADP·AlF_x structures still remained poorly defined but the minimally biased density maps clearly showed the trace of the GroES main-chain and density for several larger side-chains. Limited manual model building was performed with the O program[45] to correct small local differences in each model, while also maintaining strict NCS symmetry between the different protomers. Model quality was assessed using Ramachandran analysis and deviations from ideal geometry with the PROCHECK program.[46] At this point, all water molecules and bound ions were removed from the models, except for those in well defined electron density at the nucleotide-binding site. The models were then optimized using rigid body refinement followed by domain *B*-factor refinement in CNS, with the equatorial, intermediate, apical and GroES domains all treated as independent rigid bodies. Refinements were carried out using all the experimental data and the amplitude-based MLF maximum likelihood target function except in the case of unliganded GroEL where the MLHL target function was used since experimental phase information was available. Water molecules were then automatically located using the standard CNS task file that was modified to use map coefficients from the density modification protocol described above. Water molecules were accepted if they had a peak height of at least 1.5σ, made reasonable hydrogen bond interactions, and had a refined *B*-factor of less than 65 $Å^2$. This conservative protocol located only

well ordered water molecules or bound ions, thus minimizing the over-fitting of the diffraction data by addition of unnecessary parameters. The models generated were then input into isotropic temperature factor or TLS refinement.

Refinement with isotropic temperature factors

Isotropic temperature factor refinements were performed using REFMAC version 5.1.99[47,48] with standard scripts. All temperature factors were set to a constant value of 60 Å^2 prior to the start of refinement. Tight position NCS restraints were applied using a weight of 0.05 Å. Restraints on *B*-factors between NCS related atoms were modified to account for differences between domains in the asymmetric unit. Weights between 2.0 Å^2 and 5.0 Å^2 were used depending on the structure; the optimum value being obtained by monitoring the free *R*-value after each test refinement. Cycles of restrained coordinate and isotropic temperature factor refinement were carried out using all experimental data and the amplitude-based maximum likelihood target function. A bulk solvent model was used and an overall anisotropic scale factor was applied.

TLS refinement

TLS refinements were performed with REFMAC version 5.1.99 using standard scripts. All temperature factors were set to a constant value of 60 Å^2 prior to the start of refinement. Each domain in a GroEL subunit (equatorial, intermediate, and apical) and each GroES subunit were treated as rigid TLS groups. Test refinements with larger rigid groups, e.g. whole GroEL molecules, or rings formed of equatorial domains, produced significantly higher free *R*-values, indicating that the use of the single domain TLS decomposition was appropriate. Nucleotide molecules plus associated metal ions and water molecules were included in the equatorial rigid TLS group definition. Other water molecules and ions were not assigned to any TLS group. The upper Gly192-Gly375 and lower Pro192-Gly410 hinges were chosen as the TLS origins for the apical and intermediate domain, respectively, as these are the pivot points for the functionally relevant motions in GroEL. For the equatorial domain and GroES, the center of geometry of the domain was chosen as the origin. Cycles of TLS refinement were carried out using all experimental data and the amplitude-based maximum likelihood target function. A bulk solvent model was used and an overall anisotropic scale factor was applied. The number of cycles of TLS refinement cycles required for convergence varied from 6 to 15 depending on the structure. After TLS refinement, restrained coordinate and residual isotropic temperature factor refinement was carried out. Tight position NCS restraints were applied using a weight of 0.05 Å. *B*-factors between NCS related atoms were also tightly restrained using a weight of 0.5 Å^2.

Analysis of TLS parameters

Anisotropic displacement parameters U_{ij} were calculated using the program TLSANL[49,50] for each atom by decomposition of the TLS tensors. Coordinate files were generated with isotropic equivalent *B*-factors (B_{iso}), calculated as the trace of each atomic U_{ij}. The B_{iso} values were used to compare with the results of the isotropic refinements. The TLSANL program was also used to generate axes representing the translation, libration and screw motions. Python[51] scripts were written to process these axes for visualization in PyMOL.[52] The scripts corrected the axes for the difference in the center of reactions used in TLSANL and the TLS origins used in REFMAC. These corrected axes were then transformed by the NCS operators for each structure in order to superimpose them on a representative domain for visual analysis. An anisotropy factor for each translation and libration tensor was defined as $|\mathbf{P}_{max}|/|\mathbf{P}_{min}|$, where $\mathbf{P}_{max}$ is the magnitude of the largest principal axis of the tensor and $\mathbf{P}_{min}$ is the smallest principal axis.

Analysis of anisotropic temperature factors

Rosenfeld analyses were performed on the ADPs using ANISOANL.[36] Only main-chain atoms were used in the calculation of the difference values. Thermal ellipsoids calculated from the ADPs derived from the TLS parameters were visualized using both RASTEP[53,54] and XtalView.[55]

PDB accession codes

The atomic coordinates and structure factors for GroEL, GroEL–ATPγS, GroEL–GroES–ADP·AlF$_x$, and GroEL–GroES–ADP complexes are deposited with the Protein Data Bank under PDB codes 1SS8, 1SX3, 1SVT, and 1SX4.

Acknowledgements

This paper is dedicated to the memory of Paul B. Sigler, who initiated ideas to combine crystallography and dynamics leading to this project, and whose insight is deeply missed. We thank Mark Wilson, Martyn Winn, and Garib Murshudov for helpful discussions concerning TLS refinement, and members of the Horwich, Brunger, and Adams laboratories for useful discussions. Special thanks are extended to Ralf Grosse-Kunstleve for invaluable help with Python programs. This work was supported in part by the US Department of Energy under Contract No. DE-AC03-76SF00098 and the Howard Hughes Medical Institute (HHMI). C.C. was supported by an NSF predoctoral fellowship.

References

1. Fenton, W. A. & Horwich, A. L. (2003). Chaperonin-mediated protein folding: fate of substrate polypeptide. *Quart. Rev. Biophys.* **36**, 229–256.
2. Braig, K., Otwinowski, Z., Hegde, R., Boisvert, D. C., Joachimiak, A., Horwich, A. L. & Sigler, P. B. (1994). The crystal structure of the bacterial chaperonin GroEL at 2.8 Å. *Nature*, **371**, 578–586.
3. Fenton, W. A., Kashi, Y., Furtak, K. & Horwich, A. L. (1994). Residues in chaperonin GroEL required for polypeptide binding and release. *Nature*, **371**, 614–619.
4. Itzhaki, L. S., Otzen, D. E. & Fersht, A. R. (1995). Nature and consequences of GroEL–protein interactions. *Biochemistry*, **34**, 14581–14587.
5. Lin, Z., Schwartz, F. P. & Eisenstein, E. (1995). The hydrophobic nature of GroEL-substrate binding. *J. Biol. Chem.* **270**, 1011–1014.

6. Buckle, A. M., Zahn, R. & Fersht, A. R. (1997). A structural model for GroEL-polypeptide recognition. *Proc. Natl Acad. Sci. USA*, **94**, 3571–3575.
7. Chen, L. & Sigler, P. B. (1999). The crystal structure of a GroEL/peptide complex: plasticity as a basis for substrate diversity. *Cell*, **99**, 757–768.
8. Chandrasekhar, G. N., Tilly, K., Woolford, C., Hendrix, R. & Georgopoulos, C. (1986). Purification and properties of the groES morphogenetic protein of *Escherichia coli*. *J. Biol. Chem.* **261**, 12414–12419.
9. Gray, T. E. & Fersht, A. R. (1991). Cooperativity in ATP hydrolysis by GroEL is increased by GroES. *FEBS Letters*, **292**, 254–258.
10. Jackson, G. S., Staniforth, R. A., Halsall, D. J., Atkinson, T., Holbrook, J. J., Clarke, A. R. & Burston, S. G. (1993). Binding and hydrolysis of nucleotides in the chaperonin catalytic cycle: implications for the mechanism of assisted protein folding. *Biochemistry*, **32**, 2554–2563.
11. Todd, M. J., Viitanen, P. V. & Lorimer, G. H. (1994). Dynamics of the chaperonin ATPase cycle: implications for facilitated protein folding. *Science*, **265**, 659–666.
12. Hunt, J. F., Weaver, A. J., Landry, S. J., Gierasch, L. & Deisenhofer, J. (1996). The crystal structure of the GroES co-chaperonin at 2.8 Å resolution. *Nature*, **379**, 37–45.
13. Roseman, A. M., Chen, S., White, H., Braig, K. & Saibil, H. R. (1996). The chaperonin ATPase cycle: mechanism of allosteric switching and movements of substrate-binding domains in GroEL. *Cell*, **87**, 241–251.
14. Xu, Z., Horwich, A. L. & Sigler, P. B. (1997). The crystal structure of the asymmetric GroEL-GroES-(ADP)7 chaperonin complex. *Nature*, **388**, 741–750.
15. Chaudhry, C., Farr, G. W., Todd, M. J., Rye, H. S., Brunger, A. T.,, Adams, P. D. *et al*. (2003). Role of the gamma-phosphate of ATP in triggering protein folding by GroEL-GroES: function, structure and energetics. *EMBO J.* **22**, 4877–4887.
16. Weissman, J. S., Hohl, C. M., Kovalenko, O., Kashi, Y., Chen, S., Braig, K. *et al*. (1995). Mechanism of GroEL action: productive release of polypeptide from a sequestered position under GroES. *Cell*, **83**, 577–587.
17. Weissman, J. S., Rye, H. S., Fenton, W. A., Beechem, J. M. & Horwich, A. L. (1996). Characterization of the active intermediate of a GroEL-GroES-mediated protein folding reaction. *Cell*, **84**, 481–490.
18. Mayhew, M., da Silva, A. C., Martin, J., Erdjument-Bromage, H., Tempst, P. & Hartl, F. U. (1996). Protein folding in the central cavity of the GroEL–GroES chaperonin complex. *Nature*, **379**, 420–426.
19. Rye, H. S., Burston, S. G., Fenton, W. A., Beechem, J. M., Xu, Z., Sigler, P. B. & Horwich, A. L. (1997). Distinct actions of *cis* and *trans* ATP within the double ring of the chaperonin GroEL. *Nature*, **388**, 792–798.
20. Rye, H. S., Roseman, A. M., Chen, S., Furtak, K., Fenton, W. A., Saibil, H. R. & Horwich, A. L. (1999). GroEL-GroES cycling: ATP and nonnative polypeptide direct alternation of folding-active rings. *Cell*, **97**, 325–338.
21. Yifrach, O. & Horovitz, A. (1995). Nested cooperativity in the ATPase activity of the oligomeric chaperonin GroEL. *Biochemistry*, **34**, 5303–5308.
22. Burston, S. G., Ranson, N. A. & Clarke, A. R. (1995). The origins and consequences of asymmetry in the chaperonin reaction cycle. *J. Mol. Biol.* **249**, 138–152.
23. Ma, J. & Karplus, M. (1998). The allosteric mechanism of the chaperonin GroEL: a dynamic analysis. *Proc. Natl Acad. Sci. USA*, **95**, 8502–8507.
24. Ma, J., Sigler, P. B., Xu, Z. & Karplus, M. (2000). A dynamic model for the allosteric mechanism of GroEL. *J. Mol. Biol.* **302**, 303–313.
25. Schomaker, V. & Trueblood, K. N. (1968). On the rigid-body motion of molecules in crystals. *Acta Crystallog. sect. D*, **24**, 63–76.
26. Diamond, R. (1990). On the use of normal modes in thermal parameter refinement: theory and application to the bovine pancreatic trypsin inhibitor. *Acta Crystallog. sect. A*, **46**, 425–435.
27. Howlin, B., Moss, D. D. & Harris, G. W. (1989). Segmented anisotropic refinement of bovine ribonuclease A by the application of the rigid-body TLS model. *Acta Crystallog. sect. A*, **45**, 851–861.
28. Schwartz, T., Behlke, J., Lowenhaupt, K., Heinemann, U. & Rich, A. (2001). Structure of the DLM-1-Z-DNA complex reveals a conserved family of Z-DNA-binding proteins. *Nature Struct. Biol.* **8**, 761.
29. Papiz, M. Z., Prince, S. M., Howard, T., Cogdell, R. J. & Isaacs, N. W. (2003). The structure and thermal motion of the B800-850 LH2 complex from Rps. Acidophila at 2.0 Å resolution and 100K: new structural features and functionally relevant motions. *J. Mol. Biol.* **326**, 1523–1538.
30. Wilson, M. A. & Brunger, A. T. (2000). The 1.0 Å crystal structure of Ca^{2+}-bound calmodulin: an analysis of disorder and implications for functionally relevant plasticity. *J. Mol. Biol.* **301**, 1237–1256.
31. Matoba, Y. & Sugiyama, M. (2003). Atomic resolution structure of prokaryotic phospholipase A2: analysis of internal motion and implication for a catalytic mechanism. *Proteins: Struct. Funct. Genet.* **51**, 453–469.
32. Braig, K., Adams, P. D. & Brunger, A. T. (1995). Conformational variability in the refined structure of the chaperonin GroEL at 2.8 A resolution. *Nature Struct. Biol.* **2**, 1083–1094.
33. Boisvert, D. C., Wang, J., Otwinowski, Z., Horwich, A. L. & Sigler, P. B. (1996). The 2.4 Å crystal structure of the bacterial chaperonin GroEL complexed with ATP gamma S. *Nature Struct. Biol.* **3**, 170–177.
34. Wang, J. & Boisvert, D. C. (2003). Structural basis of GroEL-assisted protein folding from the crystal structure of (GroEL-KMgATP)14 at 2.0 Å resolution. *J. Mol. Biol.* **327**, 843–855.
35. Ranson, N. A., Farr, G. W., Roseman, A. M., Gowen, B. , Fenton, W. A., Horwich, A. L. & Saibil, H. R. (2001). ATP-bound states of GroEL captured by cryo-electron microscopy. *Cell*, **107**, 869–879.
36. Rosenfeld, R. E., Trueblood, K. N. & Dunitz, J. D. (1978). A test for rigid-body vibrations based on a generalization of Hirshfeld's "rigid-bond" postulate. *Acta Crystallog. sect. A*, **34**, 828–829.
37. Levitt, M., Sander, C. & Stern, P. S. (1985). Protein normal mode dynamics: trypsin inhibitor, crambin, ribonuclease and lysozyme. *J. Mol. Biol.* **181**, 423–447.
38. Fiaux, J., Bertelsen, E. B., Horwich, A. L. & Wuthrich, K. (2002). NMR analysis of a 900K GroEL GroES complex. *Nature*, **418**, 207–211.
39. Rye, H. S. (2001). Application of fluorescence resonance energy transfer to the GroEL-GroES chaperonin reaction. *Methods*, **24**, 278–288.
40. Berman, H. M., Westbrook, J., Feng, Z., Gilliland, G., Bhat, T. N., Weissig, H. *et al*. (2000). The Protein Data Bank. *Nucl. Acids Res.* **28**, 235–242.
41. Kleywegt, G. J. & Jones, T. A. (1999). Software for handling macromolecular envelopes. *Acta Crystallog. sect. D*, **55**, 941–944.
42. Brunger, A. T., Adams, P. D., Clore, G. M., DeLano, W. L., Gros, P., Grosse-Kunstleve, R. W.

et al. (1998). Crystallography & NMR system: a new software suite for macromolecular structure determination. *Acta Crystallog. sect. D*, **54**, 905–921.
43. Abrahams, J. P., Buchanan, S. K., Van Raaij, M. J., Fearnley, I. M., Leslie, A. G. & Walker, J. E. (1996). The structure of bovine F1-ATPase complexed with the peptide antibiotic efrapeptin. *Proc. Natl Acad. Sci. USA*, **93**, 9420–9424.
44. Abrahams, J. P. & De Graaff, R. A. (1998). New developments in phase refinement. *Curr. Opin. Struct. Biol.* **5**, 601–605.
45. Jones, T. A., Zou, J. Y., Cowan, S. W. & Kjeldgaard, M. (1991). Improved methods for building protein models in electron density maps and the location of errors in these models. *Acta Crystallog. sect. A*, **47**, 110–119.
46. Laskowski, R. A., Macarthur, M. W., Moss, D. S. & Thornton, J. M. (1993). PROCHECK: a program to check the stereochemical quality of protein structures. *J. Appl. Crystallog.* **26**, 283–291.
47. Murshudov, G. N., Vagin, A. A., Lebedev, A., Wilson, K. S. & Dodson, E. J. (1999). Efficient anisotropic refinement of macromolecular structures using FFT. *Acta Crystallog. sect. D*, **55**, 247–255.
48. Winn, M. D., Isupov, M. N. & Murshudov, G. N. (2001). Use of TLS parameters to model anisotropic displacements in macromolecular refinement. *Acta Crystallog. sect. D*, **57**, 122–133.
49. Howlin, B., Butler, S. A., Moss, D. S., Harris, G. W. & Driessen, H. P. C. (1993). TLSANL: TLS parameter-analysis program for segmented anisotropic refinement of macromolecular structures. *J. Appl. Crystallog.* **26**, 622–624.
50. Collaborative Computational Project, Number 4. (1994). The CCP4 suite: programs for protein crystallography. *Acta Crystallog. sect. D*, **50**, 760–763.
51. Lutz, M. & Ascher, D. (1999). *Learning Python*. O'Reilly and Associates, San Carlos, CA, USA.
52. DeLano, W. l. (2002). *The PyMOL Molecular Graphics System* . DeLano Scientific, San Carlos, CA, USA.
53. Merritt, E. A. & Murphy, M. E. P. (1994). Raster3D version 2.0. A program for photorealistic molecular graphics. *Acta Crystallog. sect. D*, **50**, 869–873.
54. Merritt, E. A. (1999). Expanding the model: anisotropic displacement parameters in protein structure refinement. *Acta Crystallog. sect. D*, **55**, 1109–1117.
55. McRee, D. E. (1992). A visual protein crystallographic software system for X11/Xview. *J. Mol. Graph.* **10**, 44–46.

Edited by R. Huber

(Received 13 May 2004; received in revised form 30 June 2004; accepted 9 July 2004)